



Article

# Effects of Protonation, Hydroxylamination, and Hydrazination of g-C<sub>3</sub>N<sub>4</sub> on the Performance of Matrimid<sup>®</sup>/g-C<sub>3</sub>N<sub>4</sub> Membranes

María Soto-Herranz <sup>1,\*</sup>, Mercedes Sánchez-Báscones <sup>1</sup>, Antonio Hernández-Giménez <sup>2</sup>, José I. Calvo-Díez <sup>2</sup>, Jesús Martín-Gil <sup>3</sup> and Pablo Martín-Ramos <sup>4,\*</sup>

<sup>1</sup> Department of Agroforestry Sciences, ETSIIAA, University of Valladolid, Avenida de Madrid 44, 34004 Palencia, Spain; msanchez@agro.uva.es

<sup>2</sup> SMAP, UA-UVa\_CSIC, Associated Research Unit to CSIC, Universidad de Valladolid, Paseo Belén 7, 47011 Valladolid, Spain; tonhg@termo.uva.es (A.H.-G.); jicalvo@termo.uva.es (J.I.C.-D.)

<sup>3</sup> Agriculture and Forestry Engineering Department, ETSIIAA, Universidad de Valladolid, Avenida de Madrid 44, 34004 Palencia, Spain; mgil@iaf.uva.es

<sup>4</sup> Department of Agricultural and Environmental Sciences, Instituto Universitario de Investigación en Ciencias Ambientales (IUCA), EPS, Universidad de Zaragoza, Carretera de Cuarte s/n, 22071 Huesca, Spain

\* Correspondence: maria.soto.herranz@alumnos.uva.es (M.S.-H.); pmr@unizar.es (P.M.-R.); Tel.: +34-(974)-292668 (P.M.-R.)

Received: 29 October 2018; Accepted: 4 December 2018; Published: 5 December 2018



**Abstract:** One of the challenges to continue improving polymeric membranes properties involves the development of novel chemically modified fillers, such as nitrogen-rich 2-D nanomaterials. Graphitic carbon nitride (g-C<sub>3</sub>N<sub>4</sub>) has attracted significant interest as a new class of these fillers. Protonation is known to afford it desirable functionalities to form unique architectures for various applications. In the work presented herein, doping of Matrimid<sup>®</sup> with protonated g-C<sub>3</sub>N<sub>4</sub> to yield Matrimid<sup>®</sup>/g-C<sub>3</sub>N<sub>4</sub> mixed matrix membranes was found to improve gas separation by enhancing the selectivity for CO<sub>2</sub>/CH<sub>4</sub> by up to 36.9% at 0.5 wt % filler doping. With a view to further enhancing the contribution of g-C<sub>3</sub>N<sub>4</sub> to the performance of the composite membrane, oxygen plasma and hydrazine monohydrate treatments were also assayed as alternatives to protonation. Hydroxylamination by oxygen plasma treatment increased the selectivity for CO<sub>2</sub>/CH<sub>4</sub> by up to 52.2% (at 2 wt % doping) and that for O<sub>2</sub>/N<sub>2</sub> by up to 26.3% (at 0.5 wt % doping). Hydrazination led to lower enhancements in CO<sub>2</sub>/CH<sub>4</sub> separation, by up to 11.4%. This study suggests that chemically-modified g-C<sub>3</sub>N<sub>4</sub> may hold promise as an additive for modifying the surface of Matrimid<sup>®</sup> and other membranes.

**Keywords:** carbon nitride; CO<sub>2</sub>/CH<sub>4</sub>; gas separation; Matrimid<sup>®</sup> 5218; mixed matrix membrane; O<sub>2</sub>/N<sub>2</sub>

## 1. Introduction

CO<sub>2</sub> is significantly present in mixtures where CH<sub>4</sub> is the major and valuable component. Its removal from CH<sub>4</sub> mixtures is particularly important in processes such as biogas upgrading or natural gas sweetening. Conventional industrial methods used for such CO<sub>2</sub> removal include adsorption [1], and water scrubbing and absorption [2] processes. Nonetheless, separation processes mediated by membranes can generally offer advantages over aforementioned techniques in terms of low capital cost, ease of processing, small footprint area, high energy efficiency, and ease of preparation and control [3,4].

Another closely related burgeoning field is that of oxygen production from air separation, since it can be used in many environmental applications, such as in the combustion enhancement of natural

gas or in coal gasification [5]. Although cryogenic distillation and pressure swing adsorption are the mainstream technologies for oxygen-enriched air production, the use of membranes has been deemed as specially promising.

Basu et al. [6] and Zhang et al. [7] published two reviews on membrane materials used for CO<sub>2</sub>/CH<sub>4</sub> separation. Among them, and apart from zeolite SAPO-34-based membranes [8–12], polyimides (PI) were claimed to exhibit the best combination of permeability and selectivity, thermal and chemical stability, and water resistance in biogas upgrading. In a similar fashion, glassy polyimides have also proven to exhibit excellent O<sub>2</sub>/N<sub>2</sub> selectivity [13].

The most popular commercially available PI, 3,3'-4,4'-benzophenone tetracarboxylic-dianhydride diaminophenylindane, better known as Matrimid<sup>®</sup> 5218A, has been shown to combine a remarkable gas separation performance with other desirable features in terms of solubility, processability, thermal stability, chemical resistance, adhesion, film durability, and toughness. The state-of-the-art based on this thermoplastic PI for gas separation applications has been recently covered in a thorough review by Castro-Muñoz et al. [14]. In terms of future trends to further enhance Matrimid's properties, they insisted on the need to continue developing novel chemically modified fillers as a key challenge.

Amongst two-dimensional nanomaterials that are being explored for the development of high-performance separation membranes, discussed in a recent review by Zhu et al. [15], graphitic carbon nitride (g-C<sub>3</sub>N<sub>4</sub>) has attracted significant interest as a new class of filler. This mild bandgap metal-free organic semiconductor has remarkable applications as a catalyst for environmental pollution remediation [16,17].

Theoretical studies have preconized its suitability for H<sub>2</sub> or He purification from other gases [18–21], and several experimental works have shown that it can be successfully used in the fabrication of hybrid membranes with enhanced properties. For instance, Hou et al. [22] reported a zeolitic imidazolate framework-8 (ZIF-8) hybrid membrane doped with g-C<sub>3</sub>N<sub>4</sub> nanosheets for H<sub>2</sub>/CO<sub>2</sub> separation, with an excellent selectivity. g-C<sub>3</sub>N<sub>4</sub> nanosheets were also incorporated into the matrix of polymers of intrinsic microporosity (PIM-1) by Tian et al. [23], resulting in an increase in the selectivities for H<sub>2</sub>/CH<sub>4</sub> and H<sub>2</sub>/N<sub>2</sub>.

As regards other membrane separation (non-gas) applications, Wang et al. [24] co-doped a polyamide (PA) forward osmosis membrane, based on a porous polyethersulfone substrate, with reduced graphene oxide and graphitic g-C<sub>3</sub>N<sub>4</sub>. By doing so, they obtained an osmotic water flux nearly 20% higher than that of the control membrane. Also in a PA nanofiltration membrane, modification with g-C<sub>3</sub>N<sub>4</sub> nanosheets was shown to improve the permeability, antifouling properties, hydrophilicity, negative charge density, roughness and thermal stability [25]. Similar conclusions were reached for reverse osmosis PA membranes doped with acidified g-C<sub>3</sub>N<sub>4</sub> by Gao et al. [26]. Doping g-C<sub>3</sub>N<sub>4</sub> into a sodium alginate matrix or into poly(vinyl alcohol) also improved the performance of hybrid membranes for water/ethanol separation [27,28]; and doping of g-C<sub>3</sub>N<sub>4</sub> co-impregnated with Cu<sup>+</sup> and Fe<sup>2+</sup> ions into a Pebax<sup>®</sup> membrane improved gasoline desulfurization [29].

Nonetheless, to the best of the authors' knowledge, there have been no reports on the utilization of g-C<sub>3</sub>N<sub>4</sub> as a filler for Matrimid<sup>®</sup> mixed matrix membranes (MMMs). The work presented herein addresses this literature gap by assessing the effects of protonation of g-C<sub>3</sub>N<sub>4</sub> as well as its treatment with hydrazine monohydrate and with oxygen plasma on the performance of MMMs for CO<sub>2</sub>/CH<sub>4</sub> and O<sub>2</sub>/N<sub>2</sub> separation.

## 2. Materials and Methods

### 2.1. Materials

Matrimid<sup>®</sup> 5218 polymer (CAS no. 104983-64-4) was obtained from Huntsman Chemical, Advanced Materials Americas Inc. (Los Angeles, CA, USA). Melamine cyanurate (CAS no. 37640-57-6) was supplied by Ferro-plast S.r.l. (Vimodrone, Italy) with a purity superior to 99%. *N-N*-Dimethylacetamide (DMAc; CAS no. CAS: 127-19-5; ≥99%) and hydrazine monohydrate (CAS

no. 7803-57-8; 98%) were purchased from Sigma-Aldrich (Munich, Germany). Reagents were used as received, without any further purification.

## 2.2. Methods

### 2.2.1. Synthesis of Graphitic Carbon Nitride ( $g\text{-C}_3\text{N}_4$ )

Graphitic carbon nitride was prepared by a modification of the thermal oxidation method [30], using melamine cyanurate as a starting material for the polymerization/condensation reaction [31]. The reagent was placed in a Vycor<sup>®</sup> glass vial and heated at 650 °C for 4 h under aeration, with a cooling/heating ramp of 10 °C·min<sup>-1</sup>. The resulting yellow powder was transferred to an agate mortar and ground. Subsequently, the samples were exposed to ultrasonic treatment for approximately 2 h using a Branson (FisherScientific, Hampton, NH, USA) Sonifier 450. Samples were dried in an oven at 105 °C for 24 h to remove moisture.

### 2.2.2. Synthesis of Protonated $g\text{-C}_3\text{N}_4$

Due to the presence of abundant  $\text{-C-N-}$  bonds in the  $g\text{-C}_3\text{N}_4$  framework, it can be easily protonated by HCl, resulting in a modification of the surface charge, from a negatively to positively charged (Figure 1a) [32]. The process consisted in adding 2 g of pristine  $g\text{-C}_3\text{N}_4$  sample to a 12 mL diluted 3% solution of HCl and treating it with ultrasound for 2 h. Samples were not subsequently washed. They were placed in an oven at 105 °C for approximately 24 h and were then ground.

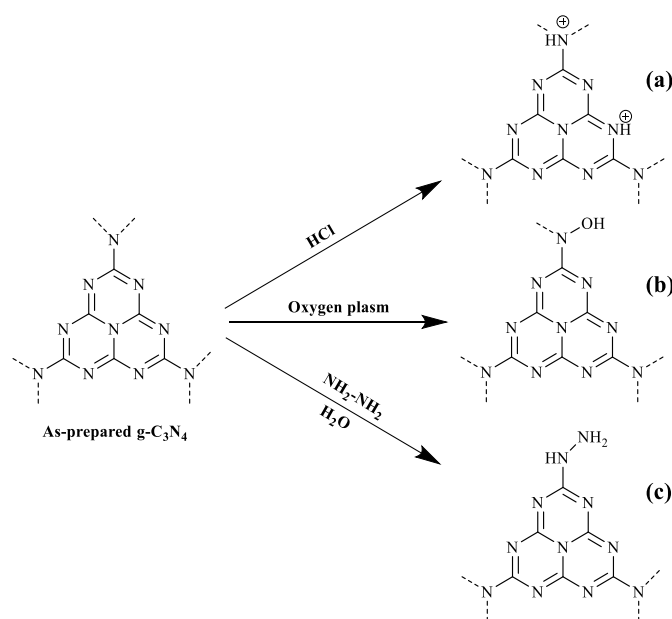


**Figure 1.** Scheme of the synthesis of: (a) protonated  $g\text{-C}_3\text{N}_4$ ; (b) oxygen plasma treatment used to introduce hydroxylamine structure (N-OH) on the surface of  $g\text{-C}_3\text{N}_4$  (hydroxylaminated  $g\text{-C}_3\text{N}_4$ ); and (c) hydrazinated  $g\text{-C}_3\text{N}_4$ .

### 2.2.3. Modifications of $g\text{-C}_3\text{N}_4$ with Oxygen Plasma and Hydrazine Monohydrate

$g\text{-C}_3\text{N}_4$  is a laminar material with non-oxidized aromatic regions and aliphatic regions containing phenolic, carboxyl, and oxygen epoxide groups that make it hydrophilic in aqueous media. This behavior can be modified through treatment with oxygen plasma or with hydrazine monohydrate.

In the former approach, interfacial forces are improved via plasma treatment, an ecologically benign process that does not produce liquid chemical residues. When the plasma is used with oxygen gas, it dissociates in order to generate oxygen-containing radicals [33], which incorporate  $\text{-OH}$ , as hydroxylamine groups, into the surface of  $g\text{-C}_3\text{N}_4$ , improving its dispersibility [34] (Figure 1b).

The oxygen plasma treatment was conducted using a Harrick Plasma (Ithaca, NY, USA) PDC-002 apparatus. 150 mg of  $g\text{-C}_3\text{N}_4$  were placed on a Petri dish on a quartz sample holder within the plasma cavity. The operating power remained at 10.2 W, the chamber pressure was 300 Torr with an  $\text{O}_2$  flow of  $35\text{ cm}^3\cdot\text{min}^{-1}$ , and the treatment time was 90 min.

In the later approach, diazanyl group modified  $g\text{-C}_3\text{N}_4\text{-NHNH}_2$  (Figure 1c) was obtained according to the procedure described by Chen et al. [35]: 1 g of as-synthesized  $g\text{-C}_3\text{N}_4$  was mixed with 20 mL water and 4 mL hydrazine hydrate, followed by stirring at  $80\text{ }^\circ\text{C}$  for 40 min.

#### 2.2.4. Preparation of the Matrimid/ $g\text{-C}_3\text{N}_4$ Mixed Matrix Membranes

The Matrimid/ $g\text{-C}_3\text{N}_4$  MMMs were prepared from a Matrimid commercial polymer solution doped with 0.5 wt % or 2 wt %  $g\text{-C}_3\text{N}_4$  loading in 5 mL of DMAc solvent at adequate concentration (6% w/v) to achieve a reasonable viscosity. Working at such  $g\text{-C}_3\text{N}_4$  loadings, previous work showed that measurable effects were obtained as compared with pristine Matrimid membranes, while much higher loadings led to an inhomogeneous distribution of  $g\text{-C}_3\text{N}_4$  across the membrane film, thus compromising the mechanical stability of the resulting membranes. After stirring until complete homogenization, all solutions were sonicated for 5 min at an amplitude of 60% in a sonicator with a work/rest period of 20 s and 10 s. Next, membranes were prepared by the casting method following the protocol described by Recio et al. [36], using a glass plate at  $25\text{ }^\circ\text{C}$ . The resulting films were dried at  $60\text{ }^\circ\text{C}$  for 24 h to complete the removal of the solvent and were then placed in a vacuum oven, where they remained at  $120\text{ }^\circ\text{C}$  for 4 hours before raising the temperature to  $180\text{ }^\circ\text{C}$  for another 4–6 h. Finally, the membranes were separated from the glass plates and their thickness was determined using a Fischer (Sindelfingen, Germany) Dualscope MP0R. All thicknesses were in the 40–60  $\mu\text{m}$  range. Three samples of each formulation were prepared, and at least two pieces of each membrane were tested. Their results were averaged, with a sample to sample variability in the usual range for laboratory prepared membranes (5–10%).

#### 2.2.5. Characterization Methods

Vibrational information of the dopant and the Matrimid/ $g\text{-C}_3\text{N}_4$  MMMs was retrieved by using a Thermo Scientific (Waltham, MA, USA) Nicolet iS50 Fourier-Transform Infrared (FTIR) spectrometer. 8–10 mm  $\varnothing$  samples were cut from the films and their transmittance was measured at room temperature in a scanning range between 410 and  $4000\text{ cm}^{-1}$ , with a  $1\text{ cm}^{-1}$  spectral resolution and 64 scans.

The morphology of the as-prepared samples was examined using field emission scanning electron microscopy (FESEM), with a FEI (Hillsboro, OR, USA) QUANTA 200F device.

Thermogravimetric analysis (TG) was used to determine the thermal and/or oxidative stability of the materials. TG experiments were performed with a Mettler Toledo (Columbus, OH, USA) DMA/SDTA 861 device, heating the samples from  $50\text{ }^\circ\text{C}$  to  $850\text{ }^\circ\text{C}$  at a heating rate of  $10\text{ }^\circ\text{C}\cdot\text{min}^{-1}$ , under a  $\text{N}_2$  flow of  $20\text{ cm}^3\cdot\text{min}^{-1}$ .

#### 2.2.6. Gas Separation Performance Measurement

The pure gas permeation tests were performed on an isochoric (constant volume, variable pressure) permeation system to measure the permeability properties of the membranes. Five pure gas species ( $\text{He}$ ,  $\text{N}_2$ ,  $\text{O}_2$ ,  $\text{CH}_4$ , and  $\text{CO}_2$ ) were applied as test gases, and the permeability and perm-selectivity of Matrimid/ $g\text{-C}_3\text{N}_4$  MMMs were evaluated. Experiments were carried out at  $35\text{ }^\circ\text{C}$  using a constant feed pressure of 3 bar. To assure constant flow of each gas tested, desired pressure was maintained during 1 h and then flow measurements were taken by using a gas flow meter.

The permeability of a given membrane was calculated from Equation (1)

$$P = \frac{Q \times L}{\Delta P \times A} \quad (1)$$

where  $P$  is the permeability in barrer ( $1 \text{ barrer} = (10^{-10} \text{ cm}^3 \text{ (STP)} \times \text{cm}) / (\text{cm}^2 \times \text{s} \times \text{cmHg})$ ),  $Q$  is the volumetric flow rate [ $\text{cm}^3 \text{ (STP)}/\text{s}$ ],  $L$  is the membrane thickness [ $\text{cm}$ ],  $\Delta P$  is the pressure difference between two sides of the membrane [ $\text{cmHg}$ ], and  $A$  is the effective membrane area [ $\text{cm}^2$ ]. The perm-selectivity  $\alpha_{A/B}$  is defined as the ratio of the permeability coefficients of two gases  $A$  and  $B$  ( $P_A$  and  $P_B$ ), according to Equation (2)

$$\alpha_{A/B} = \frac{P_A}{P_B} \quad (2)$$

### 3. Results and Discussion

#### 3.1. Vibrational Characterization

##### 3.1.1. ATR-FTIR Spectra of the Modified g-C<sub>3</sub>N<sub>4</sub> Fillers

The spectra of the protonated g-C<sub>3</sub>N<sub>4</sub> samples revealed similar characteristic features to those found in the as-prepared g-C<sub>3</sub>N<sub>4</sub>, thus confirming that the structural integrity of g-C<sub>3</sub>N<sub>4</sub> remained intact after protonation (Figure 2). Strong absorption bands could be observed in the 1200–1650 cm<sup>−1</sup> range, arising from the skeletal stretching of C–N heterocycles and comprising both trigonal (N–(C)3) (full condensation) and bridging C–NH–C units (partial condensation) [37]. This would point at a successful development of an extended C–N–C network. The broad band ranging from 3000 to 3700 cm<sup>−1</sup> was assigned to N–H and O–H stretching, due to the free amino groups and adsorbed hydroxyl species, respectively, whereas the sharp band at ca. 805 cm<sup>−1</sup> was originated from the breathing vibration of tri-*s*-triazine units [38].

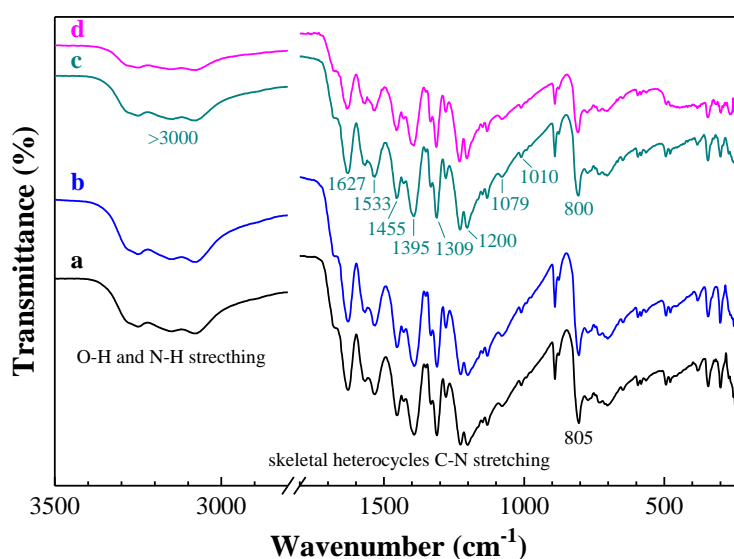


**Figure 2.** ATR-FTIR spectra of: (a) pristine g-C<sub>3</sub>N<sub>4</sub>, (b) protonated g-C<sub>3</sub>N<sub>4</sub>, (c) hydroxylaminated g-C<sub>3</sub>N<sub>4</sub>, and (d) hydrazinated g-C<sub>3</sub>N<sub>4</sub>.

After oxygen plasma treatment, all the characteristic bands were retained (Figure 2), featuring bands at 800 cm<sup>−1</sup> (assigned to the tri-*s*-triazine ring); and at 1200, 1309, 1395, 1455, 1533, and 1627 cm<sup>−1</sup> (related to C–NH–C and N–(C) stretching modes). The peaks located at 1010 cm<sup>−1</sup>, 1079 cm<sup>−1</sup>, and above 3000 cm<sup>−1</sup> corresponded to signals from N–OH groups. These results indicated that the oxygen plasma treatment led to the incorporation of N–OH on the surface of the C<sub>3</sub>N<sub>4</sub>.

The treatment of g-C<sub>3</sub>N<sub>4</sub> with hydrazine monohydrate (Figure 2) appeared to decrease the signal intensity of all peaks with respect to the original untreated g-C<sub>3</sub>N<sub>4</sub> sample or to that treated with oxygen plasma.

### 3.1.2. ATR-FTIR Spectra of Matrimid/g-C<sub>3</sub>N<sub>4</sub> MMMs

A first comparison of the spectra of pure Matrimid and of the Matrimid MMMs doped with as-prepared or protonated g-C<sub>3</sub>N<sub>4</sub> (Figure 3) evidenced shifts in the bands at 819 cm<sup>-1</sup> (shifted to 824 cm<sup>-1</sup>), 849 cm<sup>-1</sup> (to 858 cm<sup>-1</sup>), 919 cm<sup>-1</sup> (to 924 cm<sup>-1</sup>), 1475 cm<sup>-1</sup> (to 1489 cm<sup>-1</sup>), and 1606 cm<sup>-1</sup> (to 1618 cm<sup>-1</sup>). These shifts were sufficient to suggest an interaction between Matrimid and g-C<sub>3</sub>N<sub>4</sub>. As regards other strong bands in the doped samples, they were found at 708 cm<sup>-1</sup> (v(CNC) out-of-plane bending); 1090 cm<sup>-1</sup> (v(CNC) transversal stretching); 1364 cm<sup>-1</sup> (v(CNC) axial stretching); 1510 cm<sup>-1</sup> (v(C=C) aromatic stretching); 1663 cm<sup>-1</sup> (v(C=O) benzophenone carbonyl stretching); 1715 cm<sup>-1</sup> and 1784 cm<sup>-1</sup> (v(C=O) symmetric and asymmetric stretching, respectively); 2861 and 2924 cm<sup>-1</sup> (aliphatic C–H stretching); and 2958 cm<sup>-1</sup> (aromatic C–H stretching).

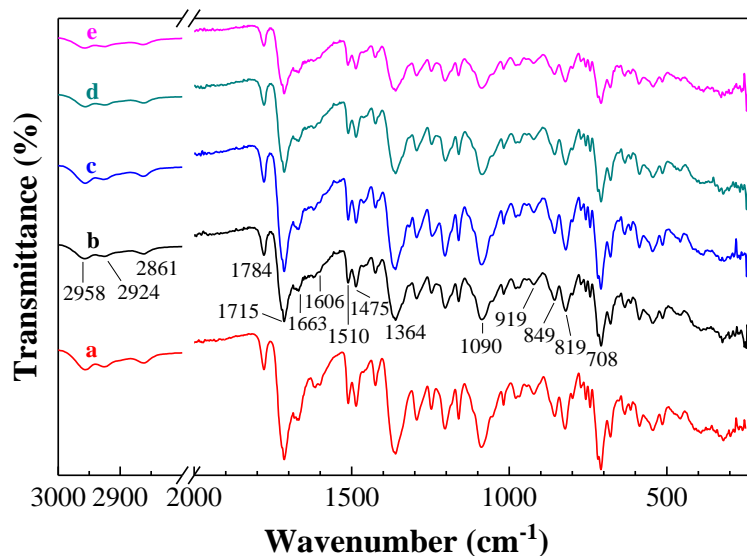


**Figure 3.** ATR-FTIR spectra of (a) a pristine Matrimid matrix and of Matrimid MMMs doped at 2 wt % with different fillers: (b) as-prepared g-C<sub>3</sub>N<sub>4</sub>, (c) protonated g-C<sub>3</sub>N<sub>4</sub>, (d) oxygen plasma-treated g-C<sub>3</sub>N<sub>4</sub>, and (e) hydrazinated g-C<sub>3</sub>N<sub>4</sub>.

Differences in the nature of the dopant, i.e., protonated vs. non-protonated g-C<sub>3</sub>N<sub>4</sub>, mainly affected the band at 1672 cm<sup>-1</sup> (amide C=O stretching), which, after protonation, was shifted to 1663 cm<sup>-1</sup>. This finding is important because it suggests that the carbonyl groups in Matrimid can act as electron acceptors from –NH<sup>+</sup> units from exfoliated protonated g-C<sub>3</sub>N<sub>4</sub>, resulting in a material assembled through electrostatic interactions (this matter will be discussed in detail in Section 3.4).

In relation to the ATR-FTIR spectra of MMMs doped with oxygen plasma and hydrazine treated g-C<sub>3</sub>N<sub>4</sub>, also depicted in Figure 3, it is worth noting that no bands associated with the N–OH or –NHNH<sub>2</sub> groups of g-C<sub>3</sub>N<sub>4</sub> (which would result from those treatments) were observed. This may be due to low dopant doses, and would be in agreement with the findings of Chen et al. [35], who reported no remarkable differences between pristine g-C<sub>3</sub>N<sub>4</sub> and g-C<sub>3</sub>N<sub>4</sub>-NHNH<sub>2</sub>. On the other hand, the band at 1606 cm<sup>-1</sup>, present in the pristine matrix, was found to disappear upon doping in both cases.

### 3.2. SEM Analysis

SEM was used to study the MMMs cross-section morphology. The micrographs of the neat Matrimid membrane (not shown) featured a smooth surface without obvious imperfections, in good agreement with those reported, for instance, by Ebadi Amooghin et al. [39].

Representative micrographs of Matrimid/g-C<sub>3</sub>N<sub>4</sub> MMMs with different g-C<sub>3</sub>N<sub>4</sub> loadings and sonication times are shown in Figure 4a–c. At low loadings (0.5 wt %, Figure 4a,b) and sonication times (30 min), the g-C<sub>3</sub>N<sub>4</sub> dopant was typically well dispersed. However, at higher loadings (e.g., 10 wt %,



Figure 4c) and moderate sonication times (4 h), several large clusters of  $g\text{-C}_3\text{N}_4$  could be found. These clusters ranged in size from 20 to 50 nm. This would be in agreement with the findings of Tian et al. [23], who evaluated the improvement of gas separation performance of mixed matrix membranes composed of PIM-1 doped with different  $g\text{-C}_3\text{N}_4$  loads as compared to pure PIM-1 membranes. They found that, using  $\text{CHCl}_3$  as a solvent and after sonication for 12 h, the  $g\text{-C}_3\text{N}_4$  dopant was well dispersed throughout the matrix at low loading levels (0.5–1 wt %), and also observed the presence of partial agglomeration for higher filler contents (>1 wt %).

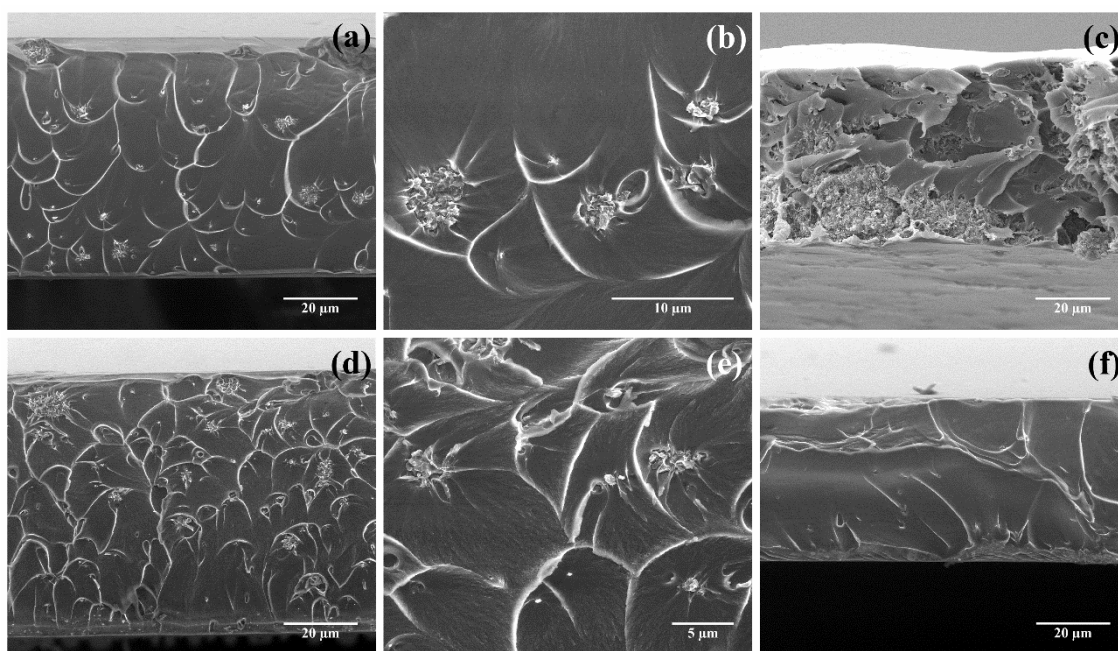


**Figure 4.** Cross-sectional SEM micrographs for MMMs doped with  $g\text{-C}_3\text{N}_4$  subjected to different treatments and prepared with different sonication times: Matrimid membrane doped with 0.5 wt % protonated  $g\text{-C}_3\text{N}_4$  at 3000 $\times$  (a) and 6000 $\times$  (b) magnification; Matrimid membrane doped with 10 wt % protonated  $g\text{-C}_3\text{N}_4$  loading after 4 hours of sonication (c) at 3000 $\times$ ; Matrimid loaded with 0.5 wt %  $g\text{-C}_3\text{N}_4$  treated with oxygen plasma at 3000 $\times$  (d) and 10000 $\times$  (e); Matrimid loaded with 0.5 wt % hydrazine monohydrate-treated  $g\text{-C}_3\text{N}_4$  at 3000 $\times$  (f). Micrographs of MMMs at 2 wt % loading were analogous to the ones at 0.5 wt %.

It is also worth noting that, in contrast with the neat Matrimid membrane, a scalloped morphology was observed for the MMMs doped with protonated  $g\text{-C}_3\text{N}_4$  (Figure 4a,b). As noted by Venna et al. [40] (and references therein), it may be attributed to the formation of elongated polymer segments with increased plastic deformation of the polymer and can be regarded as an indication of a good interaction between the polymer and the filler, further supported by the absence of a sieve-in-a-cage morphology (i.e., when there are interfacial voids larger than the penetrating molecules, so a by-pass around the particles is produced, enhancing the permeability and reducing the apparent selectivity [41]) at each loading.

SEM analysis was also conducted upon Matrimid doping with 0.5 wt % of  $g\text{-C}_3\text{N}_4$  treated with oxygen plasma (Figure 4d,e) or with hydrazine monohydrate (Figure 4f). In the hydroxylaminated  $g\text{-C}_3\text{N}_4$ -doped samples, one could observe a crater-like pattern in which the eye of each crater was formed by nanosized fillers, similar to that obtained for protonated  $g\text{-C}_3\text{N}_4$ , albeit more evident. The filler also appeared to be uniformly distributed along the polymer matrix. According to Ebadi Amooghin et al. [39], such crater-like morphology of MMMs arises from an adequate compatibility existing between two phases, possibly due to the interfacial stress concentrations because of the polymer matrix/filler consecutive debonding. Thus, this deformation of the polymer matrix was again indicative of a strong interaction of polymer chains and filler. On the other hand, the MMMs doped

with hydrazinolyzed  $g\text{-C}_3\text{N}_4$  did not show a significant modification of the smooth aspect of pristine Matrimid, thus suggesting a weaker interaction.

### 3.3. Studies on Thermal Stability of the Matrimid/ $g\text{-C}_3\text{N}_4$ Membranes

The thermal stability of the Matrimid/ $g\text{-C}_3\text{N}_4$  membranes was evaluated in comparison to pristine Matrimid (Figure 5). The thermograms showed that all the studied membranes were stable up to 470 °C and that only a small weight loss was observed between 200 °C and 250 °C (see Table 1), which could be attributed to residual solvent evaporation (the boiling point of DMAc is 202–204 °C). The inflection point for this first stage occurred at 351 °C for pristine Matrimid, and at lower temperatures for the MMMs membranes: 295 °C for Matrimid loaded with protonated  $g\text{-C}_3\text{N}_4$ , 247 °C for Matrimid doped with oxygen plasma-treated  $g\text{-C}_3\text{N}_4$ , and 287 °C for Matrimid with hydrazine-treated  $g\text{-C}_3\text{N}_4$ . Above 450 °C, a decomposition in two stages took place, with inflection points at around 517 °C and 591 °C (for pristine Matrimid they appeared at 518 °C and 580 °C, respectively). This second weight loss could be ascribed to the evolution of CO, CO<sub>2</sub>, and CH<sub>4</sub> from the cleavage of the benzene ring pattern of the Matrimid matrix. Degradation of the Matrimid/ $g\text{-C}_3\text{N}_4$  composites ended at 850 °C after a brief carbonization process.

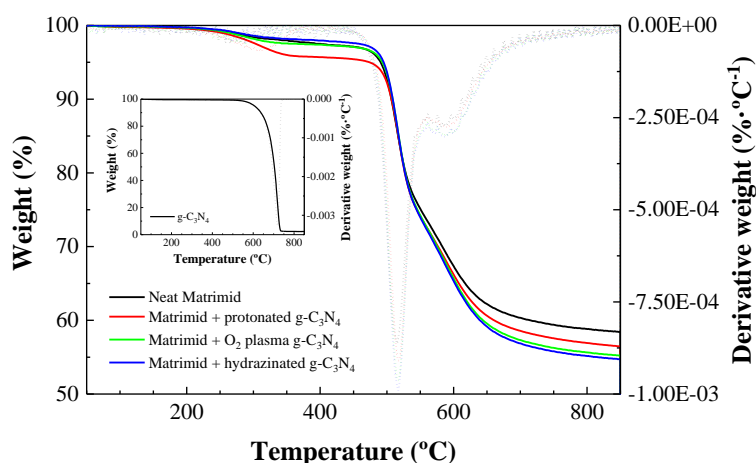


**Figure 5.** TG (solid line,  $y$ -axis on the left side of the graph) and DTG (dashed line,  $y$ -axis on the right side of the graph) curves for neat Matrimid and Matrimid-based membranes doped with 0.5 wt % of protonated  $g\text{-C}_3\text{N}_4$ , hydroxylaminated  $g\text{-C}_3\text{N}_4$ , and hydrazinated  $g\text{-C}_3\text{N}_4$ . The inset shows the TG/DTG curves for the untreated  $g\text{-C}_3\text{N}_4$  filler.

**Table 1.** TG curves features for neat Matrimid, the  $g\text{-C}_3\text{N}_4$  filler and the three MMMs under study

Pristine Matrimid		$g\text{-C}_3\text{N}_4$		Protonated $g\text{-C}_3\text{N}_4$		Oxygen Plasma-Treated $g\text{-C}_3\text{N}_4$		Hydrazinated $g\text{-C}_3\text{N}_4$	
Weight Loss (%)	Midpoint (°C)	Weight Loss (%)	Midpoint (°C)	Weight Loss (%)	Midpoint (°C)	Weight Loss (%)	Midpoint (°C)	Weight Loss (%)	Midpoint (°C)
2.8	287			4.2	29.4	2.70	284	2.2	280
23.4	516	97.6	700	23.3	518	24.8	518	25.9	517
14.9	609			15.9	611	17.0	611	17.1	611

Taking in account the delayed TG inflection points for MMMs vs. neat Matrimid at around 591 °C (588 °C for Matrimid/hydrazinated  $g\text{-C}_3\text{N}_4$ ; 589 °C for Matrimid/hydroxylaminated  $g\text{-C}_3\text{N}_4$  and 593 °C for Matrimid/protonated  $g\text{-C}_3\text{N}_4$  vs. 580 °C for pristine Matrimid, as shown in Figure 5), it may be inferred that thermally stable structures were created in the membrane matrix after treatment with either  $g\text{-C}_3\text{N}_4(\text{N-OH})$  or  $g\text{-C}_3\text{N}_4(\text{N-H}^+)$ .



### 3.4. CO<sub>2</sub>/CH<sub>4</sub> and O<sub>2</sub>/N<sub>2</sub> Gas Separation Performance of Matrimid/g-C<sub>3</sub>N<sub>4</sub> MMMs

Apropos of the pristine Matrimid membrane, the CO<sub>2</sub>/CH<sub>4</sub> selectivity value was within the range reported in other recent works (34.2 [42], 34.9 [43], 35.7 [44], 36.3 [45]), and so was the O<sub>2</sub>/N<sub>2</sub> selectivity (6.5–6.8 [42,46,47]).

Doping of the Matrimid MMMs with protonated g-C<sub>3</sub>N<sub>4</sub> particulates at 0.5 wt % increased the CO<sub>2</sub>/CH<sub>4</sub> selectivity by 36.9% (from 36.3 to 49.6) as compared to the neat Matrimid membrane, although the O<sub>2</sub>/N<sub>2</sub> selectivity decreased by 5.7% (from 7.0 to 6.6). Doping at 2 wt % led to a lower increase in the CO<sub>2</sub>/CH<sub>4</sub> selectivity (by 16.5%, from 36.3 to 42.2), but the O<sub>2</sub>/N<sub>2</sub> selectivity was preserved (Table 2).

**Table 2.** Permeabilities/selectivities of the Matrimid/g-C<sub>3</sub>N<sub>4</sub> MMMs for He, N<sub>2</sub>, O<sub>2</sub>, CH<sub>4</sub>, CO<sub>2</sub>, O<sub>2</sub>/N<sub>2</sub>, and CO<sub>2</sub>/CH<sub>4</sub> as a function of different filler treatments at different doping levels (0.5 wt % and 2 wt %)

MMM	Permeability (Barrer)					Selectivity		Ref.
	He	N <sub>2</sub>	O <sub>2</sub>	CH <sub>4</sub>	CO <sub>2</sub>	O <sub>2</sub> /N <sub>2</sub>	CO <sub>2</sub> /CH <sub>4</sub>	
Matrimid (control)	22.00	0.27	1.90	0.24	8.70	7.0	36.3	[48]
Matrimid/protonated g-C <sub>3</sub> N <sub>4</sub> 0.5 wt %	23.53	0.26	1.70	0.15	7.69	6.6	49.6	This study
Matrimid/protonated g-C <sub>3</sub> N <sub>4</sub> 2 wt %	20.17	0.20	1.44	0.15	6.45	7.1	42.2	This study
Matrimid/hydroxylaminated g-C <sub>3</sub> N <sub>4</sub> 0.5 wt %	24.12	0.19	1.71	0.21	7.86	8.9	37.9	This study
Matrimid/hydroxylaminated g-C <sub>3</sub> N <sub>4</sub> 2 wt %	23.63	0.23	1.69	0.13	7.15	7.2	55.2	This study
Matrimid/hydrazinated g-C <sub>3</sub> N <sub>4</sub> 0.5 wt %	20.60	0.20	1.44	0.17	6.56	7.1	39.0	This study
Matrimid/hydrazinated g-C <sub>3</sub> N <sub>4</sub> 2 wt %	18.65	0.20	1.36	0.15	6.19	6.8	40.4	This study

The behavior for the MMMs doped with oxygen plasma-treated g-C<sub>3</sub>N<sub>4</sub> treatment as a function of the filler doping values was the opposite: doping at 2 wt % led to a larger increase in the CO<sub>2</sub>/CH<sub>4</sub> selectivity (by 52.2%, from 36.3 to 55.2) than doping at 0.5 wt % (4.4% increase). On the other hand, doping at 0.5 wt % led to a significant enhancement of O<sub>2</sub>/N<sub>2</sub> selectivity (26.3% increase, from 7.0 to 8.9), while the increase for 2 wt % doping was only 2.7%.

In relation to the hydrazine treatment, it enhanced CO<sub>2</sub>/CH<sub>4</sub> selectivities (by 7.5% and by 11.4% for 0.5 wt % and 2 wt % doping, respectively), while O<sub>2</sub>/N<sub>2</sub> separation values remained similar to those of the Matrimid matrix (0.7% and −3.7% variation).

The results in the two latter treatments would be in agreement with observations by other authors, such as Tian et al. [23], who synthesized MMMs with a PIM matrix doped with g-C<sub>3</sub>N<sub>4</sub>, and an increase in the permeability values was observed as the filler concentration was increased to reach >1 wt %.

The enhancement of gas separation in the Matrimid membranes after doping with modified g-C<sub>3</sub>N<sub>4</sub> may be referred either to an increase of hydrogen bonding in the Matrimid/g-C<sub>3</sub>N<sub>4</sub> composite structure or to cross-linking modifications in Matrimid mediated by g-C<sub>3</sub>N<sub>4</sub>.

The first hypothesis suggests that the good results obtained for Matrimid MMMs doped with protonated g-C<sub>3</sub>N<sub>4</sub> would be referred to, on the one hand, their exfoliated nature and the associated surface gain for interaction, and, on the other hand, to the presence of −NH<sup>+</sup> groups capable of bonding, through hydrogen bonding, with the carbonyl groups of the Matrimid matrix. The benzene rings of both g-C<sub>3</sub>N<sub>4</sub> and Matrimid would lend themselves to the formation of “π-staking” (Figure 6a).

In the case of g-C<sub>3</sub>N<sub>4</sub> treated with oxygen plasma, designed to provide hydroxylamine N–OH groups that would bond with the carbonyl groups of Matrimid, it is unclear whether interactions between filler and matrix would be mediated by subsequent hydrogen bonding between such groups. There is also the possibility of formation of charge transfer between the −OH (behaving as electron acceptor group) and the aromatic nucleus in Matrimid (behaving as an electron donor group), as depicted in Figure 6b.

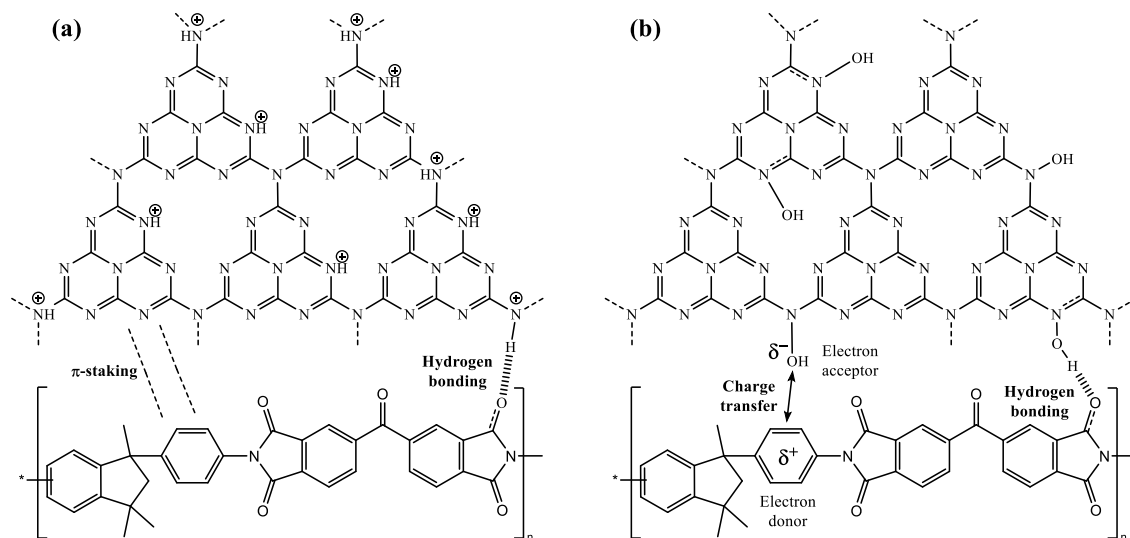


**Figure 6.** (a) Linking modes between protonated g-C<sub>3</sub>N<sub>4</sub> and Matrimid; (b) a possible linking mode between oxygen plasma-treated g-C<sub>3</sub>N<sub>4</sub> and Matrimid.

In the case of Matrimid/hydrazinated g-C<sub>3</sub>N<sub>4</sub> MMM, its behavior can be associated to a potential cross-linking effect of the g-C<sub>3</sub>N<sub>4</sub>(NH–NH<sub>2</sub>) filler. Addition of H<sub>2</sub>N–R–NH<sub>2</sub> fillers has been reported to lead to cross-linking modification of polyimides [49], increasing chain packing and inhibiting the intra-segmental and inter-segmental mobilities of the matrix, resulting in higher gas selectivity [50]. For instance, *p*-phenylenediamine (PPD) was reported to be a good cross-linking agent for Matrimid, showing a remarkable enhancement of selectivity for O<sub>2</sub>/N<sub>2</sub> as compared to the unmodified membrane (from 6.2 to 10.0 due to the affinity of nitrogen-containing molecules towards oxygen) [13]. Thus, the hydrazinated g-C<sub>3</sub>N<sub>4</sub> discussed herein could be regarded as an alternative to PPD, albeit the associated enhancement of gas selectivity for O<sub>2</sub>/N<sub>2</sub> would be lower.

#### 4. Conclusions

Modified g-C<sub>3</sub>N<sub>4</sub> was assessed as a filler for the doping of Matrimid matrices with a view to enhancing their gas separation properties. The resulting Matrimid/g-C<sub>3</sub>N<sub>4</sub> MMMs were characterized through ATR-FTIR vibrational analysis, SEM microscopy, thermal analysis techniques, and gas perm-selectivity assays. Due to the strong interfacial interactions among the modified g-C<sub>3</sub>N<sub>4</sub> and the Matrimid matrix, the hybrid nanocomposite membranes featured high swelling resistance and mechanical stability. In the assays presented herein, the doping of Matrimid with modified g-C<sub>3</sub>N<sub>4</sub> led to an enhancement of CO<sub>2</sub>/CH<sub>4</sub> selectivity—as compared to that of the pure Matrimid membrane—in all cases. In particular, MMMs doped with 0.5 wt % protonated g-C<sub>3</sub>N<sub>4</sub> and with 2 wt % hydroxylaminated g-C<sub>3</sub>N<sub>4</sub> showed the best CO<sub>2</sub>/CH<sub>4</sub> separation performances (with an increase by 36.9% and 52.2% vs. neat Matrimid, respectively). On the other hand, doping with 0.5 wt % oxygen plasma-treated g-C<sub>3</sub>N<sub>4</sub> improved the O<sub>2</sub>/N<sub>2</sub> selectivity by 26.3%, as compared to pristine Matrimid. Thus, the chemical modification of g-C<sub>3</sub>N<sub>4</sub> may hold promise as an efficient pathway toward the doping of Matrimid and other membranes.

**Author Contributions:** Conceptualization, A.H.-G., J.M.-G., and P.M.-R.; Data curation, M.S.-H.; Formal analysis, M.S.-H., J.M.-G., and P.M.-R.; Funding acquisition, M.S.-B., A.H.-G., and J.I.C.-D.; Investigation, M.S.-H., J.M.-G., and P.M.-R.; Methodology, A.H.-G. and J.M.-G.; Resources, A.H.-G., J.I.C.-D., and J.M.-G.; Supervision, M.S.-B., A.H.-G., and J.M.-G.; Validation, J.M.-G. and P.M.-R.; Visualization, M.S.-H. and P.M.-R.; Writing—original draft, M.S.-H., J.M.-G., and P.M.-R.; Writing—review & editing, M.S.-H. and P.M.-R.

**Funding:** This research was funded by the European Union, project LIFE+ AMMONIA TRAPPING (LIFE15-ENV/ES/000284); and by Spanish MINECO, projects MAT2016-76413-C2-R1 and MAT2016-76413-C2-R2. The APC was funded by LIFE+ AMMONIA TRAPPING (LIFE15-ENV/ES/000284) project.

**Acknowledgments:** The authors would like to gratefully acknowledge Manuel Avella-Romero for the SEM characterization at the Microscopy Facilities of the University of Valladolid; Cristina Álvarez and Ángel Emilio Lozano for the thermal characterization carried out at ICTP-CSIC; and Sara Rodríguez for the gas separation measurements. The guidance and help provided by Carla Aguilar-Lugo is also acknowledged. P.M.-R. acknowledges the financial support of Santander Universidades through “Becas Iberoamérica. Santander Investigación—Santander Universidades, España” program.

**Conflicts of Interest:** The authors declare no conflict of interest.

## References

1. Drioli, E.; Romano, M. Progress and new perspectives on integrated membrane operations for sustainable industrial growth. *Ind. Eng. Chem. Res.* **2001**, *40*, 1277–1300. [[CrossRef](#)]
2. Tuinier, M.J.; van Sint Annaland, M.; Kramer, G.J.; Kuipers, J.A.M. Cryogenic CO<sub>2</sub> capture using dynamically operated packed beds. *Chem. Eng. Sci.* **2010**, *65*, 114–119. [[CrossRef](#)]
3. Brunetti, A.; Sun, Y.; Caravella, A.; Drioli, E.; Barbieri, G. Process intensification for greenhouse gas separation from biogas: More efficient process schemes based on membrane-integrated systems. *Int. J. Greenh. Gas Control* **2015**, *35*, 18–29. [[CrossRef](#)]
4. Dorosti, F.; Omidkhah, M.; Abedini, R. Fabrication and characterization of Matrimid/MIL-53 mixed matrix membrane for CO<sub>2</sub>/CH<sub>4</sub> separation. *Chem. Eng. Res. Des.* **2014**, *92*, 2439–2448. [[CrossRef](#)]
5. Burdyny, T.; Struchtrup, H. Hybrid membrane/cryogenic separation of oxygen from air for use in the oxy-fuel process. *Energy* **2010**, *35*, 1884–1897. [[CrossRef](#)]
6. Basu, S.; Khan, A.L.; Cano-Odena, A.; Liu, C.; Vankelecom, I.F.J. Membrane-based technologies for biogas separations. *Chem. Soc. Rev.* **2010**, *39*, 750–768. [[CrossRef](#)]
7. Zhang, Y.; Sunarso, J.; Liu, S.; Wang, R. Current status and development of membranes for CO<sub>2</sub>/CH<sub>4</sub> separation: A review. *Int. J. Greenh. Gas Control* **2013**, *12*, 84–107. [[CrossRef](#)]
8. Carreon, M.A.; Li, S.; Falconer, J.L.; Noble, R.D. Alumina-supported SAPO-34 membranes for CO<sub>2</sub>/CH<sub>4</sub> separation. *J. Am. Chem. Soc.* **2008**, *130*, 5412–5413. [[CrossRef](#)]
9. Carreon, M.A.; Li, S.; Falconer, J.L.; Noble, R.D. SAPO-34 seeds and membranes prepared using multiple structure directing agents. *Adv. Mater.* **2008**, *20*, 729–732. [[CrossRef](#)]
10. Li, S.; Carreon, M.A.; Zhang, Y.; Funke, H.H.; Noble, R.D.; Falconer, J.L. Scale-up of SAPO-34 membranes for CO<sub>2</sub>/CH<sub>4</sub> separation. *J. Membr. Sci.* **2010**, *352*, 7–13. [[CrossRef](#)]
11. Li, S. SAPO-34 membranes for CO<sub>2</sub>/CH<sub>4</sub> separation. *J. Membr. Sci.* **2004**, *241*, 121–135. [[CrossRef](#)]
12. Falconer, J.L.; Carreon, M.A.; Li, S.; Noble, R.D. Synthesis of Zeolites and Zeolite Membranes Using Multiple Structure Directing Agents. U.S. Patent 8,302,782 B2, 6 November 2012.
13. Aziz, F.; Ismail, A.F. Preparation and characterization of cross-linked Matrimid<sup>®</sup> membranes using para-phenylenediamine for O<sub>2</sub>/N<sub>2</sub> separation. *Sep. Purif. Technol.* **2010**, *73*, 421–428. [[CrossRef](#)]
14. Castro-Muñoz, R.; Martín-Gil, V.; Ahmad, M.Z.; Fila, V. Matrimid<sup>®</sup> 5218 in preparation of membranes for gas separation: Current state-of-the-art. *Chem. Eng. Commun.* **2017**, *205*, 161–196. [[CrossRef](#)]
15. Zhu, J.; Hou, J.; Uliana, A.; Zhang, Y.; Tian, M.; Van der Bruggen, B. The rapid emergence of two-dimensional nanomaterials for high-performance separation membranes. *J. Mater. Chem. A* **2018**, *6*, 3773–3792. [[CrossRef](#)]
16. Mamba, G.; Mishra, A.K. Graphitic carbon nitride (g-C<sub>3</sub>N<sub>4</sub>) nanocomposites: A new and exciting generation of visible light driven photocatalysts for environmental pollution remediation. *Appl. Catal. B* **2016**, *198*, 347–377. [[CrossRef](#)]
17. Ding, F.; Yang, D.; Tong, Z.; Nan, Y.; Wang, Y.; Zou, X.; Jiang, Z. Graphitic carbon nitride-based nanocomposites as visible-light driven photocatalysts for environmental purification. *Environ. Sci. Nano* **2017**, *4*, 1455–1469. [[CrossRef](#)]
18. De Silva, S.W.; Du, A.; Senadeera, W.; Gu, Y. Strained graphitic carbon nitride for hydrogen purification. *J. Membr. Sci.* **2017**, *528*, 201–205. [[CrossRef](#)]
19. Ji, Y.; Dong, H.; Lin, H.; Zhang, L.; Hou, T.; Li, Y. Heptazine-based graphitic carbon nitride as an effective hydrogen purification membrane. *RSC Adv.* **2016**, *6*, 52377–52383. [[CrossRef](#)]
20. Li, F.; Qu, Y.; Zhao, M. Efficient helium separation of graphitic carbon nitride membrane. *Carbon* **2015**, *95*, 51–57. [[CrossRef](#)]
21. Qu, Y.; Li, F.; Zhao, M. Theoretical design of highly efficient CO<sub>2</sub>/N<sub>2</sub> separation membranes based on electric quadrupole distinction. *J. Phys. Chem. C* **2017**, *121*, 17925–17931. [[CrossRef](#)]

22. Hou, J.; Wei, Y.; Zhou, S.; Wang, Y.; Wang, H. Highly efficient H<sub>2</sub>/CO<sub>2</sub> separation via an ultrathin metal-organic framework membrane. *Chem. Eng. Sci.* **2018**, *182*, 180–188. [[CrossRef](#)]
23. Tian, Z.; Wang, S.; Wang, Y.; Ma, X.; Cao, K.; Peng, D.; Wu, X.; Wu, H.; Jiang, Z. Enhanced gas separation performance of mixed matrix membranes from graphitic carbon nitride nanosheets and polymers of intrinsic microporosity. *J. Membr. Sci.* **2016**, *514*, 15–24. [[CrossRef](#)]
24. Wang, Y.; Ou, R.; Wang, H.; Xu, T. Graphene oxide modified graphitic carbon nitride as a modifier for thin film composite forward osmosis membrane. *J. Membr. Sci.* **2015**, *475*, 281–289. [[CrossRef](#)]
25. Chen, J.; Li, Z.; Wang, C.; Wu, H.; Liu, G. Synthesis and characterization of g-C<sub>3</sub>N<sub>4</sub> nanosheet modified polyamide nanofiltration membranes with good permeation and antifouling properties. *RSC Adv.* **2016**, *6*, 112148–112157. [[CrossRef](#)]
26. Gao, X.; Li, Y.; Yang, X.; Shang, Y.; Wang, Y.; Gao, B.; Wang, Z. Highly permeable and antifouling reverse osmosis membranes with acidified graphitic carbon nitride nanosheets as nanofillers. *J. Mater. Chem. A* **2017**, *5*, 19875–19883. [[CrossRef](#)]
27. Cao, K.; Jiang, Z.; Zhang, X.; Zhang, Y.; Zhao, J.; Xing, R.; Yang, S.; Gao, C.; Pan, F. Highly water-selective hybrid membrane by incorporating g-C<sub>3</sub>N<sub>4</sub> nanosheets into polymer matrix. *J. Membr. Sci.* **2015**, *490*, 72–83. [[CrossRef](#)]
28. Wang, J.; Li, M.; Zhou, S.; Xue, A.; Zhang, Y.; Zhao, Y.; Zhong, J.; Zhang, Q. Graphitic carbon nitride nanosheets embedded in poly(vinyl alcohol) nanocomposite membranes for ethanol dehydration via pervaporation. *Sep. Purif. Technol.* **2017**, *188*, 24–37. [[CrossRef](#)]
29. Ding, H.; Pan, F.; Mulalic, E.; Goma, H.; Li, W.; Yang, H.; Wu, H.; Jiang, Z.; Wang, B.; Cao, X.; et al. Enhanced desulfurization performance and stability of Pebax membrane by incorporating Cu<sup>+</sup> and Fe<sup>2+</sup> ions co-impregnated carbon nitride. *J. Membr. Sci.* **2017**, *526*, 94–105. [[CrossRef](#)]
30. Niu, P.; Zhang, L.; Liu, G.; Cheng, H.-M. Graphene-Like Carbon Nitride Nanosheets for Improved Photocatalytic Activities. *Adv. Funct. Mater.* **2012**, *22*, 4763–4770. [[CrossRef](#)]
31. Dante, R.C.; Martín-Ramos, P.; Sánchez-Arévalo, F.M.; Huerta, L.; Bizarro, M.; Navas-Gracia, L.M.; Martín-Gil, J. Synthesis of crumpled nanosheets of polymeric carbon nitride from melamine cyanurate. *J. Solid State Chem.* **2013**, *201*, 153–163. [[CrossRef](#)]
32. Ong, W.-J.; Tan, L.-L.; Chai, S.-P.; Yong, S.-T.; Mohamed, A.R. Surface charge modification via protonation of graphitic carbon nitride (g-C<sub>3</sub>N<sub>4</sub>) for electrostatic self-assembly construction of 2D/2D reduced graphene oxide (rGO)/g-C<sub>3</sub>N<sub>4</sub> nanostructures toward enhanced photocatalytic reduction of carbon dioxide to methane. *Nano Energy* **2015**, *13*, 757–770. [[CrossRef](#)]
33. Park, O.-K.; Young Kim, W.; Min Kim, S.; You, N.-H.; Jeong, Y.; Su Lee, H.; Ku, B.-C. Effect of oxygen plasma treatment on the mechanical properties of carbon nanotube fibers. *Mater. Lett.* **2015**, *156*, 17–20. [[CrossRef](#)]
34. Bu, X.; Li, J.; Yang, S.; Sun, J.; Deng, Y.; Yang, Y.; Wang, G.; Peng, Z.; He, P.; Wang, X.; et al. Surface modification of C<sub>3</sub>N<sub>4</sub> through oxygen-plasma treatment: A simple way toward excellent hydrophilicity. *ACS Appl. Mater. Interfaces* **2016**, *8*, 31419–31425. [[CrossRef](#)] [[PubMed](#)]
35. Chen, Y.; Lin, B.; Wang, H.; Yang, Y.; Zhu, H.; Yu, W.; Basset, J.-M. Surface modification of g-C<sub>3</sub>N<sub>4</sub> by hydrazine: Simple way for noble-metal free hydrogen evolution catalysts. *Chem. Eng. J.* **2016**, *286*, 339–346. [[CrossRef](#)]
36. Recio, R.; Lozano, Á.E.; Prádanos, P.; Marcos, Á.; Tejerina, F.; Hernández, A. Effect of fractional free volume and T<sub>g</sub> on gas separation through membranes made with different glassy polymers. *J. Appl. Polym. Sci.* **2008**, *107*, 1039–1046. [[CrossRef](#)]
37. Dong, F.; Zhao, Z.; Xiong, T.; Ni, Z.; Zhang, W.; Sun, Y.; Ho, W.-K. In situ construction of g-C<sub>3</sub>N<sub>4</sub>/g-C<sub>3</sub>N<sub>4</sub> metal-free heterojunction for enhanced visible-light photocatalysis. *ACS Appl. Mater. Interfaces* **2013**, *5*, 11392–11401. [[CrossRef](#)] [[PubMed](#)]
38. Zhang, Y.; Mori, T.; Niu, L.; Ye, J. Non-covalent doping of graphitic carbon nitride polymer with graphene: Controlled electronic structure and enhanced optoelectronic conversion. *Energy Environ. Sci.* **2011**, *4*, 4517. [[CrossRef](#)]
39. Ebadi Amooghini, A.; Omidkhan, M.; Kargari, A. The effects of aminosilane grafting on NaY zeolite–Matrimid<sup>®</sup>5218 mixed matrix membranes for CO<sub>2</sub>/CH<sub>4</sub> separation. *J. Membr. Sci.* **2015**, *490*, 364–379. [[CrossRef](#)]

40. Venna, S.R.; Lartey, M.; Li, T.; Spore, A.; Kumar, S.; Nulwala, H.B.; Luebke, D.R.; Rosi, N.L.; Albenze, E. Fabrication of MMMs with improved gas separation properties using externally-functionalized MOF particles. *J. Mater. Chem. A* **2015**, *3*, 5014–5022. [[CrossRef](#)]
41. Zornoza, B.; Casado, C.; Navajas, A. Advances in hydrogen separation and purification with membrane technology. In *Renewable Hydrogen Technologies*; Gandía, L.M., Arzamendi, G., Diéguez, P.M., Eds.; Elsevier: Amsterdam, The Netherlands, 2013; pp. 245–268.
42. Shao, L.; Liu, L.; Cheng, S.-X.; Huang, Y.-D.; Ma, J. Comparison of diamino cross-linking in different polyimide solutions and membranes by precipitation observation and gas transport. *J. Membr. Sci.* **2008**, *312*, 174–185. [[CrossRef](#)]
43. Loloie, M.; Omidkhah, M.; Moghadassi, A.; Amooghin, A.E. Preparation and characterization of Matrimid<sup>®</sup> 5218 based binary and ternary mixed matrix membranes for CO<sub>2</sub> separation. *Int. J. Greenh. Gas Control* **2015**, *39*, 225–235. [[CrossRef](#)]
44. Rahmani, M.; Kazemi, A.; Talebnia, F.; Abbasszadeh Gamali, P. Fabrication and characterization of brominated Matrimid<sup>®</sup> 5218 membranes for CO<sub>2</sub>/CH<sub>4</sub> separation: Application of response surface methodology (RSM). *e-Polymers* **2016**, *16*, 481–492. [[CrossRef](#)]
45. Ebadi Amooghin, A.; Omidkhah, M.; Sanaeepur, H.; Kargari, A. Preparation and characterization of Ag<sup>+</sup> ion-exchanged zeolite-Matrimid<sup>®</sup>5218 mixed matrix membrane for CO<sub>2</sub>/CH<sub>4</sub> separation. *J. Energy Chem.* **2016**, *25*, 450–462. [[CrossRef](#)]
46. Sterescu, D.M.; Stamatialis, D.F.; Wessling, M. Boltorn-modified polyimide gas separation membranes. *J. Membr. Sci.* **2008**, *310*, 512–521. [[CrossRef](#)]
47. Clausi, D.T.; Koros, W.J. Formation of defect-free polyimide hollow fiber membranes for gas separations. *J. Membr. Sci.* **2000**, *167*, 79–89. [[CrossRef](#)]
48. Tejero, R.; Lozano, Á.E.; Álvarez, C.; de Abajo, J. Synthesis, characterization, and evaluation of novel polyhydantoins as gas separation membranes. *J. Polym. Sci. Part A Polym. Chem.* **2013**, *51*, 4052–4060. [[CrossRef](#)]
49. Yong, W.F.; Li, F.Y.; Chung, T.-S.; Tong, Y.W. Highly permeable chemically modified PIM-1/Matrimid membranes for green hydrogen purification. *J. Mater. Chem. A* **2013**, *1*, 13914–13925. [[CrossRef](#)]
50. Xiao, Y.; Chung, T.; Guan, H.; Guiver, M. Synthesis, cross-linking and carbonization of co-polyimides containing internal acetylene units for gas separation. *J. Membr. Sci.* **2007**, *302*, 254–264. [[CrossRef](#)]



© 2018 by the authors. Licensee MDPI, Basel, Switzerland. This article is an open access article distributed under the terms and conditions of the Creative Commons Attribution (CC BY) license (<http://creativecommons.org/licenses/by/4.0/>).